# Development of SiC Devices for Diagnostics and Control of Combustion Products in Energy Plant Environments

Final Technical Report
Reporting Period:
October 1, 2001 to September 30, 2003

Ruby N. Ghosh and Peter Tobias

December 2003

DOE Award Number: DE-FG26-01NT41358

Center for Sensor Materials
2167 Biomedical Physical Sciences Building
Michigan State University

ABSTRACT

A sensor based on the wide bandgap semiconductor, silicon carbide (SiC), has been developed for the detection of combustion products in power plant environments. The sensor is a catalytic gate field effect device that can detect hydrogen containing species in chemically reactive, high temperature environments. The response of these metal/insulator/SiC (MISiC) devices to reducing gases has been assumed to be due to the reduction in the metal work function at the metal/oxide interface that shifts the capacitance to lower voltages. From *in-situ* capacitance-voltage measurements taken under sensor operating conditions we have discovered that two independent mechanisms are responsible for the sensor response to hydrogen and oxygen. We present a model of the device response based on the chemically induced shift of the metal/semiconductor barrier height as well as the passivation and creation of charged states at the $SiO_2$/SiC interface. The latter mechanism is much slower than the barrier height shift. Preliminary photoemission experiments have been performed to independently monitor the contribution of the two phenomena. We discuss in detail the effect of these results on sensor design and the choice of operating point for high temperature operation.

TABLE OF CONTENTS



LIST(S) OF GRAPHICAL MATERIALS

## 1. INTRODUCTION

Emissions control for the energy sector requires gas sensors that can operate in chemically reactive high temperature environments for both real time monitoring and feedback control of exhaust products. Gaseous species that need to be monitored include hydrogen, hydrocarbons, nitrogen oxides and sulfur oxides. Metal / insulator / semiconductor structures with catalytically active gates are widely used to electronically detect the presence of various chemical species [Spetz 2001]. The wide bandgap semiconductor silicon carbide, SiC, enables device operation to temperatures in excess of 1200K. In the case of the 6H polytype the energy gap is 3.0 eV, compared to 1.1 eV for silicon. These field-effect devices require a robust dielectric to enable modulation of the semiconductor carrier concentration via an applied gate potential. SiC has a native oxide, $SiO_2$, which fulfills this need. In addition SiC is chemically stable in reactive environments making it well suited for sensing applications in harsh environments.

The operation of field-effect devices is dominated by electronic interactions at interfaces. In the case of a metal/insulator/SiC (MISiC) structure these interfaces are the environment/metal interface, the metal/oxide interface and the oxide/semiconductor interface. In this report we describe how reducing and oxidizing species modify the electronic interfacial properties of $Pt/SiO_2/SiC$ devices at high temperature. These results are obtained by *in-situ* capacitance-voltage (C-V) spectroscopy performed under sensor operating conditions.

Refractory metal gate SiC devices have been demonstrated for high temperature chemical sensing application by a number of groups [Spetz 2001, Filippov 1999, Hunter 2000, Kim 2001, Nakagomi 2001, Samman 2000, Serina 2001, Ghosh 2002]. These include hydrogen and hydrocarbon sensors operating at temperatures from 600K to 1300K. Specific sensor configurations have achieved millisecond time response and sensitivity at the 0.1% level. In addition there are preliminary indications that suitably designed devices may offer sensitivity to ammonia, carbon monoxide, nitrogen oxides and fluorocarbons. For this technology to fulfill its potential in real world applications the issues of reliability and stability need to be addressed, which requires a detailed experimental study of hydrogen transduction following dehydrogenation at the heated catalytic gate.

A schematic of our catalytic gate SiC field-effect sensor for hydrogen containing species is shown in Figure I.1. Refractory metal gates such as Pt, Pd and Ir can efficiently dehydrogenate long chain hydrocarbons at temperatures above 700K. Following dehydrogenation at the heated gate, hydrogen diffuses into the structure. For a Si based catalytic gate sensor operating below 500K it has been shown that hydrogen gives rise to a polarized layer at the metal/oxide interface [Lundstrom 1976]. This chemically induced polarization charge results in a simple lateral shift of the C-V or current-voltage (I-V) characteristic of the capacitor or Schottky diode sensor, respectively. The magnitude of the voltage shift in these Si based sensors is a measure of the chemically modified metal/semiconductor barrier height. It has been assumed that the same mechanism describes the operation of higher temperature SiC based sensors for hydrogen containing species. At temperatures above 700K the diffusion time for hydrogen through 100 nm of Pt and 50 nm of $SiO_2$ is less than 5 μs [Katsuta 1979] and 0.5 ms [Beadle 1985] respectively. We demonstrate via *in-situ* C-V spectroscopy of

Pt/$SiO_2$/SiC sensors at 800K that oxidizing species affect the electronic properties of both the metal/oxide and oxide/semiconductor interfaces.

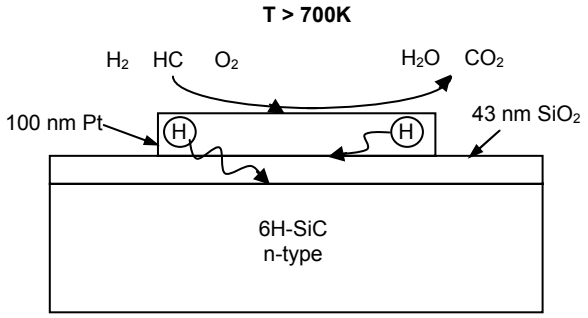


**Fig. I.1** Schematic of a catalytic gate SiC field-effect sensor for hydrogen containing gases. Typical operation is at T > 700K. Hydrogen can diffuse to both the metal/oxide and oxide/semiconductor interfaces.

## 2. EXECUTIVE SUMMARY

A silicon carbide (SiC) based sensor for the detection of power plant combustion products has been developed. The sensor is a catalytic gate field effect device that can detect hydrogen containing species in chemically reactive, high temperature environments. We describe in this report (1) the process used to fabricate the MISiC devices, (2) the spectroscopic techniques used to characterize the electronic and chemical properties of the sensor operating in high temperature hydrogen and oxygen gases, (3) the results of our experiments on the sensor response mechanisms and (4) the optimal device operating point for sensor operation.

$Pt/SiO_2/SiC$ devices were fabricated on commercially purchased single crystal wafers. Sputtering and electron beam evaporation techniques were developed to deposit the metallic platinum sensing layer that can withstand repeated cycling to 900 K without delamination. The quality of the oxide/SiC interface was characterized via capacitance – voltage spectroscopy at temperatures up to 800K in hydrogen and oxygen. The density of charged states at the oxide/SiC interface of our devices is comparable to state of the art electronic devices with standard metal gates, typically aluminum or poly-silicon. These results verify that the Pt gate does not adversely affect the electronic properties of our field-effect sensors.

The response of MISiC devices to reducing gases has been previously assumed to be due to the reduction in the metal work function at the metal/oxide interface that shifts the capacitance to lower voltages. This interpretation is based on measurements made on lower temperature ($T < 475K$) silicon sensors. We developed the capabilities to perform *in-situ* capacitance-voltage (C-V) measurements under sensor operating conditions, up to 800K. From the C-V and sensor measurements we have discovered that the sensor response to hydrogen and oxygen is due to two independent phenomena. These are the chemically induced shift of the metal/semiconductor barrier height and the passivation and creation of charged states at the $SiO_2/SiC$ interface. We have developed a model for the device response based on these two mechanisms. The time constant for charge transport in and out of the interface states was found to be several orders of magnitude slower than the barrier height shift. For optimal sensor operation the device should be biased such that the effect of the chemically induced barrier shift dominates. Our results are applicable to field-effect SiC devices in general, independent of the specifics of sample fabrication. In terms of device response time and sensor - to - sensor reliability, we find that the optimum set point for MISiC sensors is at midgap.

We developed a photoemission technique to independently monitor the effects of hydrogen and oxygen on the metal/oxide and oxide/semiconductor interfaces. A quartz sample cell for high temperature spectroscopy was fabricated. Micro-welding techniques were developed to fabricate an array of resistive micro-heaters to heat the SiC sensor. Mounted inside an ultra-violet spectrometer we will be able to monitor the device photocurrent as a function of temperature and gas composition. The gate leakage current of the MISiC devices were characterized, because the photoemission experiments require devices with low leakage currents. From preliminary photoemission measurements we find that the photocurrent increases with increasing photon energy in accordance with theory. We are in the process of analyzing the data and performing additional

experiments to determine the metal/semiconductor barrier height as a function of hydrogen concentration at various temperatures.

3. EXPERIMENTAL

### *3.1 Samples*

For our high temperature sensors, we prepare silicon carbide based metal-insulator-semiconductor devices (MISiCs) as capacitors. The cross section of the finished capacitors is shown in Fig. 3.1.1. The SiC wafers are obtained commercially from Cree, Inc [Cree]. The thermal oxide is prepared by Cree, Inc. or by the group of J. Cooper at Purdue University. The oxide is grown at Cree in dry oxygen at 1470 K [Lipkin 1996], and at Purdue in wet oxygen at 1420 K, followed at both locations by a wet anneal at 1220 K. The samples are then sawed into 1 cm x 1 cm pieces. While being sawed, the samples are protected with photoresist that is afterwards removed with Nanostrip©. The sample are then covered with photoresist only on the front side, the back oxide is etched off in buffered hydrogen fluoride solution, and the photoresist is removed with Nanostrip©. All chemicals used are CMOS grade.

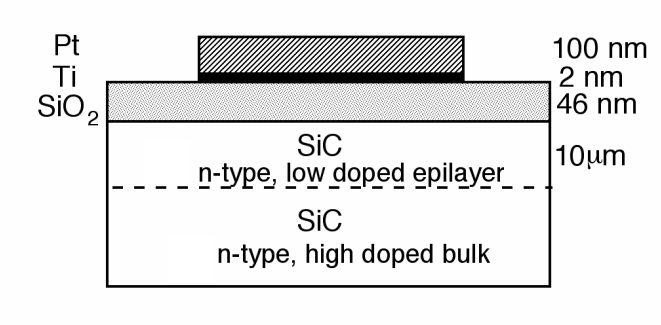


**Fig 3.1.1** Schematic cross section of the MISiC capacitor. Pt is deposited on a thermally oxidized SiC substrate with dot diameters from 200 to 1000 μm. Some samples had an intermediate layer of Ti. The Pt thickness was 100 nm for the sensor and capacitance measurement; for photoemission measurements the Pt thicknesses was 15 to 20 nm.

### *3.2 Oxide thicknesses by ellipsometry*

To measure the oxide thickness of our samples, we use a spectroscopic ellipsometer, from J. A. Woollam Co., Inc., with the material constants from Palik [1985]. The samples are cleaned with isopropanol, and the front side is blown dry. We position the sample that the elliptical light spot is parallel to one of its edges and has maximal area while still hitting only the sample surface. The measured values of delta and phi are evaluated through a model of SiO2 on SiC; the thickness of the SiO2 is fitted to the measurement values by least squares. The software estimates the precision of the inferred oxide thickness to 1 nm.

The first measurement is taken in the middle of the sample followed by two measurements in the upper and lower half, respectively. Then the sample is rotated by 90 degrees around the vertical axis, and another three measurements are taken in the same fashion. One measurement is repeated by letting the light come from the opposite direction of the first time, the thicknesses of this control measurement were within 0.2 nm of the first thickness. For most of our samples, the measured thickness was between 45 and 51 nm.

### *3.3 Sample cleaning before metal deposition*

The interface between the metal and the insulator is critical both for gas sensing and for metal adhesion, which is important for sensor reliability. To get a sharp and reproducible interface, we cleaned the sample prior to metal deposition by the RCA method: We clean the samples in a solution of conc. $NH_3$, 30%-$H_2O_2$ and $H_2O$ (1:1:6) at 75 °C for 20 min and, after rinsing with distilled water, then in a solution of conc. HCl, 30%-$H_2O_2$ and $H_2O$ (1:1:7) at 75 °C for another 20 min. At the end, the samples are rinsed with distilled water and left in the water until metal deposition. The chemicals used for cleaning are from T.J. Baker, CMOS grade.

### *3.4 Deposition of thin metal films*

After being thoroughly rinsed and blown dry with nitrogen, metal dots are deposited on the front side of the samples through a shadow mask at a temperature of 600 - 650 K. The metal thickness is ~100 nm for the capacitance and sensor measurements and ~15 nm for the photoemission samples. We have used three types of shadow masks with dot areas from $3.1 \times 10^{-8}$ up to $1.6 \times 10^{-5}$ $m^2$, giving us arrays of 20 to 50 sensors per SiC chip. The metal was deposited by either e-beam evaporation or sputtering in argon at a pressure of 0.33 Pa. The e-beam evaporated films consist of a single layer of platinum. The sputtered films are either platinum or platinum on top of a 2 nm thick titanium intermediate layer. The precision of the thickness monitors in the deposition chambers is checked in regular intervals with a Dektak profilometer. Each dot is the gate of a metal-insulator-silicon carbide capacitor (MISiC).

Scanning electron micrographs of the films (Fig. 3.4.1) show a smooth surface with grains that are on the order of the film thickness. Cycling the films to 1000K under atmospheric conditions did not result in delamination. Adhesion of the sensing metal gate is essential for long term stability of the devices.

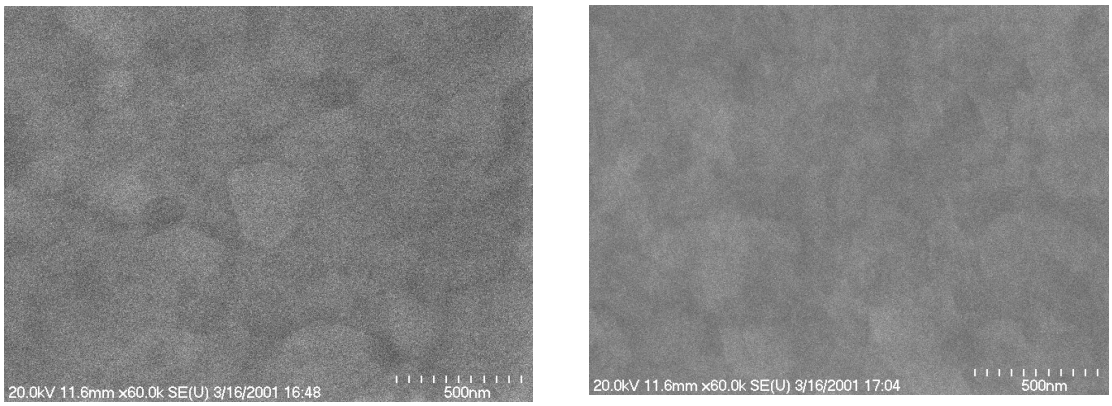


100 nm sputtered Pt

100 nm e-beam Pt

**Fig 3.4.1** SEM- pictures of deposited Pt films. Pt thickness is 100 nm and the deposition temperature is between 600 and 650 K. During the sputter deposition, a 2 nm Ti film was sputtered before the Pt. In both cases the films are smooth, with grain sizes of 100 - 200 nm.

### *3.5 Sample mounting*

Each SiC sample is mounted on a thermally conducting, but electrically insulating alumina header as shown in Fig. 3.5.1. The header provides a carrier to mount the sample in either the furnace tube for high temperature capacitance measurements or the photoemission spectrometer. In addition the header has a number of gold pads for making contact to the Pt gates and the leads to the measurement equipment. The headers are made from alumina with dimensions 24 x 9 x 0.25 mm. Gold pads are defined on the top surface using thick film technology to 15 μm. The SiC sample is attached to the alumina header with conducting glue. The conducting glue [silverprint] is thinly distributed on the middle of the header, and the sample with its back is placed on the glue. The sample is then pressed with the sharp ends of tweezers against the header to make the glue layer as thin as possible while still being continuous. The glue is cured for one hour in air at room temperature and another hour in air at 400 K. The cured glue is electrically conducting and can withstand temperatures in air up to 1000 K. The electrical connections from the different gold pads to the gates are made by bonding a thin gold wire (25 μm) from the pads to the gates at a temperature of about 600 K, with a bonding machine from Kulicke and Soffa. Fig. 3.5.1 shows a mounted sample with the electrical connections between sample and gold pads.

Electrical characterization of the samples was performed on either on a regulated hot chuck in air or in a furnace with a controlled gas atmosphere. On the hot chuck, electrical contact to the gold pads on the alumina header was made with micro-positioner controlled tungsten probe tips. In the furnace, probe tips do not work reliably, probably because of the low spring forces at high temperatures. Instead, an additional gold wire was bonded to the gold pad. The far end of the gold wire was then glued to a short piece of platinum wire, which in turn was spotwelded to the wire that forms the center conductor of the coaxial cable leading out of the furnace, Fig. 3.5.2. By using the home made high temperature coaxial leads, our measurement system allows for four-terminal electrical measurements with better than pA and pF sensitivity up to temperatures of 870 K.

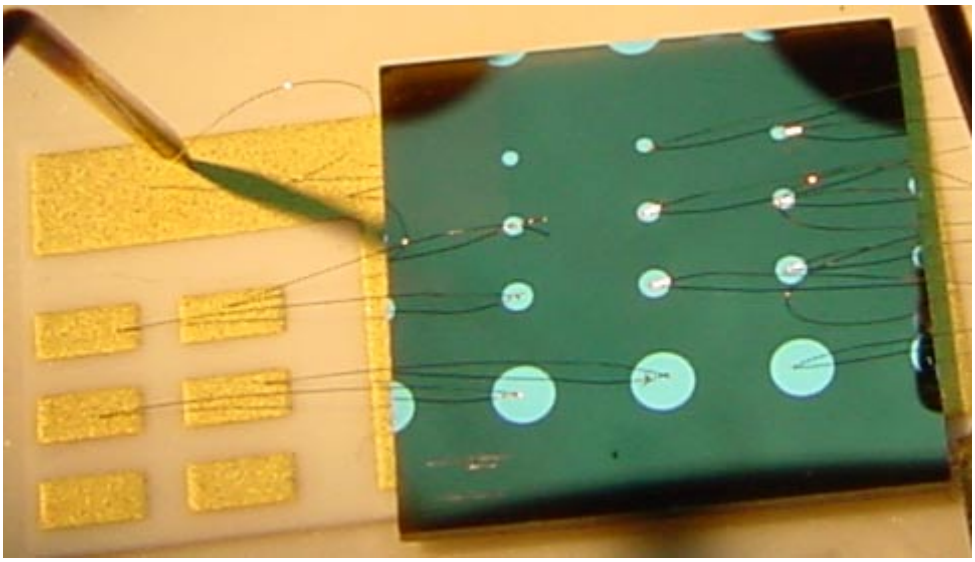

**Fig 3.5.1** SiC sample (green) mounted on alumina header with gold pads, prior to high temperature measurements. The sample is a square with 10 mm side length and contains an array of Pt gate capacitors (metallic dots).

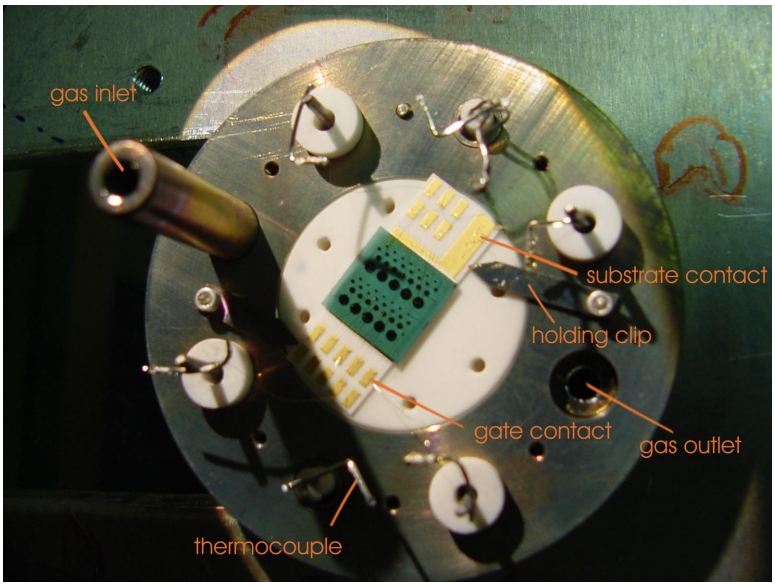


**Fig 3.5.2** Array of sensors mounted for measurements at high temperatures in the furnace. The SiC sample is glued on the alumina header, see Fig 3.5.1, held to the white ceramic surface by two clips. In this set-up, we can simultaneously contact three sensors, with the forth lead used as a ground contact. The measurement system allows for four-terminal electrical measurements with better than pA and pF sensitivity up to temperatures of 870 K.

### *3.6 C-V spectroscopy*

We have used simultaneous measurements of the high frequency capacitance and "quasi-static" capacitance to study the charge distribution of our metal / insulator / SiC capacitors. For a given applied gate voltage, the resultant electric field in the capacitor depletes the semiconductor of mobile charges, which results in a so-called space charge region in the semiconductor. As shown in Fig. 3.6.1 the MISiC device can be described as a series combination of the oxide and semiconductor capacitances, $C_{ox}$ and $C_s$ respectively. The simultaneous 1 MHz and quasi static capacitance - voltage measurements were made with a Keithley 590 high-frequency meter and a 595 quasi-static meter. The sweep velocity of the bias voltage determines the quasi-static frequency

During a sweep of the gate bias voltage from accumulation to depletion and beyond, the Fermi energy ($E_F$) is swept from the conduction band edge across the band gap towards the valence band. Interface states in the band gap in an energy width kT around $E_F$, can respond to the change of the voltage. Their capacitance, $C_i$, contributes to the low frequency capacitance of the whole sample as indicated in Fig. 3.6.1. The interface states can not contribute to the high frequency capacitance, because their charging and discharging time is too slow to follow the high frequency signal. Cooper [Cooper 1977] has developed an activated energy model of the time response of charged states at the SiC/oxide interface. The interface state response time depends on the energy of the state with respect to the conduction band ($E_C$ - E) and the temperature of the sample. At fixed temperature and a given quasi-static and high frequency probe signal, states above a minimum energy cannot react to the high frequency signal, while states below a maximum energy can react to the low frequency signal. Therefore, from the difference in the capacitance at the two frequencies, we get information about interface state density ($D_{IT}$) between the minimum and maximum energy. This technique for determining $D_{IT}$ is known as the hi-low method. Due to lack of other studies on SiC, we have taken the energy limits from Cooper's work on p-type SiC and corrected it for the different effective mass of electrons, because we use n-type SiC.

At temperatures above 500 K, we find that it is experimentally difficult to use the hi-low technique to determine $D_{IT}$. This is due to the increase in gate leakage current, > 1 pA, with increasing temperature. Although we are able to measure quasi-static curves up to 600K, random spikes in the gate current make the characteristics very noisy, rendering it difficult to obtain reproducible interface state density measurements using the hi-low techniques. Note that in Figure 4.1.3, at a gate bias of 2V the quasi-static capacitance is off scale due to a current spike. Despite the problems with the quasi-static measurements, we are able to obtain reproducible high-frequency C-V curves at temperatures up to 800K, which is well within the range of operation for catalytic gate field-effect sensors.

The high frequency data alone can be used to obtain the interface state density at the oxide/semiconductor interface is the high-frequency using techniques developed by Terman [ Terman 1962]. Note that the sensor response is also obtained from the high-frequency C-V curves in different gas environments. In the Terman technique a C-V characteristic is measured at a frequency high enough that the interface states can not follow the small AC modulation. It is assumed that they can, however, follow the slow

DC bias sweep. During the DC sweep, states in an energy range kT across from $E_F$ are charged or discharged, resulting in a stretch-out of the C-V curve. A theoretical C-V curve in the absence of interface states is calculated, which requires accurate knowledge of the semiconductor doping density as a function of position from the oxide/semiconductor interface. $D_{IT}$ is then obtained by comparing the experimental C-V characteristic to theory. Since the analysis requires computing the slope of the semiconductor potential versus capacitance curve, it is advantageous to increase the number of measurement points.

Hi-low analysis is a significantly more accurate method of determining the energy dependence of $D_{IT}$ than the Terman technique. However, in SiC devices at high temperature, where hi-low analysis is not possible due to finite gate leakage currents, Terman analysis allows us to estimate the interface state density to within an order of magnitude.

To compute $D_{IT}$ from the C-V curves, our coworker Sally Ejakov has written a MATLAB program. The block diagram of the program is shown in Fig. 3.6.2: after entering the parameter of the measurements and loading the measurement data, the program leads the user through some fitting procedures by eye and then computes the $D_{IT}$ and the energy window, in which the computed $D_{IT}$ values are valid, according to the model from Cooper [1997]. Computation of the quasi-static $D_{IT}$ is straightforward. The Terman method, however, relies on the derivative of the measured C-V curve, so to reduce the influence of noise, the measurement data are first approximated by a smooth function. Without the smoothing, the $D_{IT}$ obtained from the Terman analysis was very noisy.

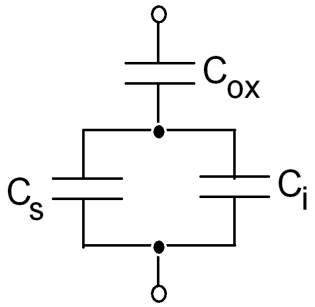


**Fig 3.6.1** Schematic representation of the different capacitances in a MISiC capacitor. $C_{ox}$ is the capacitance of the silicon dioxide, $C_s$ is the capacitance of the space charge region in the SiC, which is depleted of mobile charges, and $C_i$ is the capacitance due to states at the silicon oxide - silicon carbide interface. The interface state capacitance only contributes to the low frequency C-V measurement.

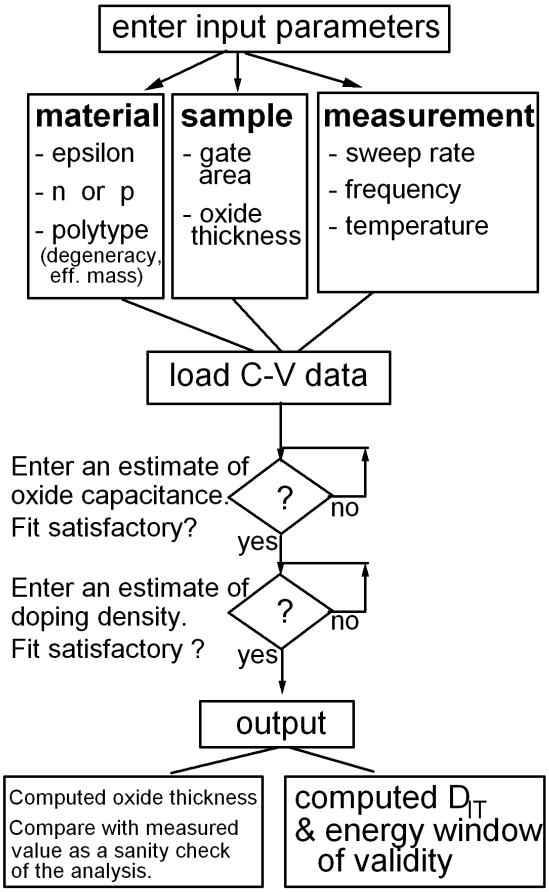


**Fig 3.6.2** Block diagram of the Matlab program that was used to compute the interface state density, $D_{IT}$. After entering the parameters and loading the measurement data, the program runs through two loops to fit an oxide capacitance and a doping density to the data. The program can compute the $D_{IT}$ either by a quasi-static analysis (HiLo) or by the Terman method.

### *3.7 Sensor measurements*

The sensors were characterized by measuring the 1 MHz capacitance in different gases. During the sensor measurement the gas environment around the sensor was varied while holding the device capacitance constant. This keeps the Fermi level at the $SiO_2$-SiC interface fixed and should minimize charging and discharging interface states. The gate voltage required to maintain the preset capacitance was monitored as the sensor signal. The gases used are nitrogen (purity 99.999%), 10% hydrogen in nitrogen (99.999%), and 1% oxygen in nitrogen (99.99%). The concentrations of the gases are chosen to reach saturated sensor signals, but to avoid explosive gas mixtures. The exposures of the MISiCs to hydrogen and oxygen are separated by short exposures to pure nitrogen, to avoid dangerous mixtures of hydrogen and oxygen in the sensor environment.

The sensor array is mounted as shown in Fig. 3.5.2 and inserted into a quartz tube that can be heated up in the furnace. We estimate the time needed for a total exchange of gases to be longer than a minute, i.e. we cannot measure fast sensor responses with the furnace set-up. On the other hand, the furnace has smaller temperature gradients than the microheaters (described in Sec. 3.9), which allows a more precise temperature control.

We use a LabView program that was written for us by Nate Verhanovitz for making the sensor measurements. The user defines a preset capacitance at the start of the measurement sequence. The program adjusts the sample bias voltage using a feedback circuit to maintain the capacitance at the desired value. For the feedback, the program compares the measured capacitance with the desired capacitance and multiplies the difference with a constant factor. The resulting product is added to the old value of the bias voltage to give the new bias voltage, which brings the capacitance closer to the desired value.

### *3.8 Spectrometer set-up*

The photoemission measurements were made using a Fluorolog-3 spectrometer from Instruments S.A., Inc. As described in section, 4.5 our experiments require excitation by deep ultra violet (UV) photons. The excitation optics consists of a 150W ozone-generating Xe lamp that has a spectrum starting at 200 nm (6.2 eV). The system includes a single Czerny-Turner excitation spectrometer with a 1200g/mm ruled grating blazed at 250nm and a single Czerny-Turner emission spectrometer with a 1200g/mm ruled grating blazed at 250 nm. A Si photodiode continuously monitors the lamp signal. Reflected light is collected by a multi-alkali photo multiplier tube (Hamamatsu R928) with photon counting electronics. Data processing was done by the Datamax (version 2.2) software package supplied with the instrument. The program records three signals simultaneously: the Si diode output (to monitor the incident photon flux), the photo multiplier output (to monitor the reflected photon flux) and the photocurrent itself. The photocurrent is read by an additional CTI card that fed the values into the Datamax program.

A Newport 1815-C Power meter with and 818 UV Silicon detector was used to monitor the Xe lamp intensity at all used wavelengths before the measurements. After an

initial warm up time of half an hour, the lamp was found to have a stable output power better than +/- 5% for a period of several hours. With the combination of a 500 micrometer pinhole and the photodiode, we have measured the lateral distribution of light intensity at the location of a device under test, see Fig. 3.8.1. The power measurements allow us to normalize our photocurrent data to the number of photons incident on the sample. In the future, to correct for the number of reflected photons, we plan to use the analyzing arm of the spectrometer with the photomultiplier tube.

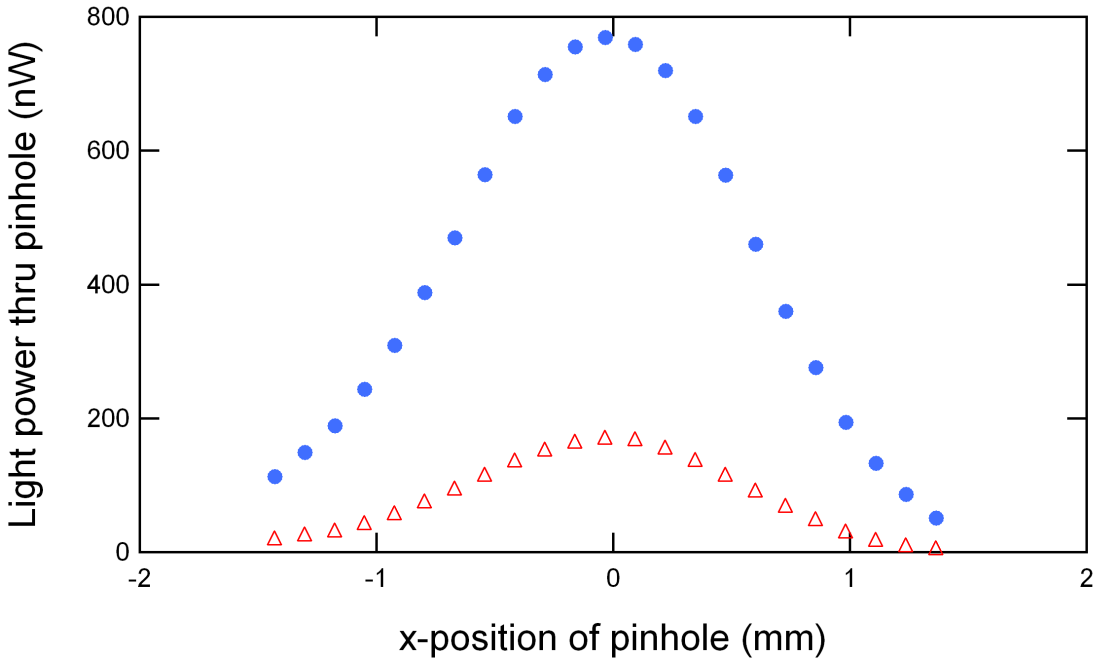


**Fig 3.8.1** The output of the UV spectrometer at the location of the sample is calibrated with a 500 um pinhole and a subsequent silicon photodiode. The wavelength was 240 nm, the bandpass of the spectrometer either 2 nm (●) or 1 nm (△).

### *3.9 Sample mounting for photoemission*

A photoemission measurement of the MISiC sensors requires a sample cell that can fulfill three demands: a free access to the sample for UV light, a controlled temperature and a controlled gas atmosphere. We have designed and built two cells that incorporate all three criteria, see Fig. 3.9.1.

We control the sample's temperature with three microheaters, from Heraeus, size 9.5 x 1.5 mm that are glued with silverpaste on the back of the alumina headers, Fig. 3.9.2. The curing process for the silverpaste is the same as on the front side. The microheaters allow us to locally heat the SiC sample up to 900 K, while the rest of the quartz cell, a few millimeters away, remains at much lower temperatures. To minimize temperature gradients in the sample, the three heaters are mounted with 1.5 mm distance and are electrically connected in parallel instead of in series to avoid a hot spot in the middle. The sample itself is single crystalline silicon carbide with an excellent heat conduction, which makes the temperature distribution on the sample surface more homogenous.

The electrical connections to the heater wires are made with a parallel gap resistance micro-joining technique, using a Unibond II system from Unitek Equipment. The copper electrodes had fixed 0.15 mm electrode spacing; the system was operated in feedback mode with the force set at 200 units and a welding time of 39 ms. The welding parameters for the two different Pt wire combinations were:

Pt (0.09 mm) to Pt (0.125 mm) – 1.2 V applied bias

Pt (0.125 mm) to Pt (0.25 mm) – 1.1 V applied bias

One wire of each heater is welded to a 10 mil Pt-wire, the second wire of the heater is welded to a short 5 mil Pt-wire that is then covered with electrically insulating silica tubing and welded to the other 10 mil Pt-wire. Three additional welds to another 5 mil Pt-wire help to keep the silica tubing in place. Figure 3.9.2 show the mounted heater assembly

On some alumina headers, we also welded thermocouples to monitor the sample temperature. Welding of the thermocouples turned out to be very difficult. Their detected temperatures became significantly lower than the temperature of the sample above 800 K. In the calibration measurements, the resistance of the heaters seemed to be a better measure of the actual sample temperature.

The assigned MISiC device is glued on the front side of the alumina header with silverpaste, and bonding connections are made from the gold pads to the gates. To some selected pads a gold wire is bonded with a loose end, to become the contact to the outside. The sample is mounted in the cell by folding the Pt-wires in the silica sleeving around the other side of the gas outlet into the cell, which is heat resistant quartz, see Fig. 3.9.3. The 10 mil Pt-heater wires are connected to the outside by spotwelding them to two piece of Pt-wire that had been in turn spotwelded to copper wires (15 mil) in the sample cell. The bond wires with open ends are wrapped around gold plated pins, from microtech, Inc., that are fixed in the sample cell. Each wrapping is secured with a little drop of silverpaste. The other end of each pin is soldered to Cu-wires (10 mil).

The cell is made gas tight by clamping its two parts together with a rubber O-ring in between. The upper part of cell consists of glass; the lower part consists of quartz. A

standard 10 mm square Spectrosil quartz fluorimeter cell from Starna Cells was used for its fabrication. In the spectrometer, the cell is standing upright, see Fig. 3.9.4. The gate under test is positioned along the diagonal of the cell to allow for its fine positioning in the light beam, see Fig. 3.8.1. We can control the position using visible light and a dentist mirror to observe the device under test. The quartz sample cell itself is mounted in a metal support structure that allows for x-y-z-phi positioning, optimizing the photon collection. The desired gas enters the sample cell through the outlet, on which the sample sits, and then leaves again flowing upwards. The entire quartz cell and support structure is housed inside an optically dark spectrometer compartment with provisions for both gas and electrical feed throughs.

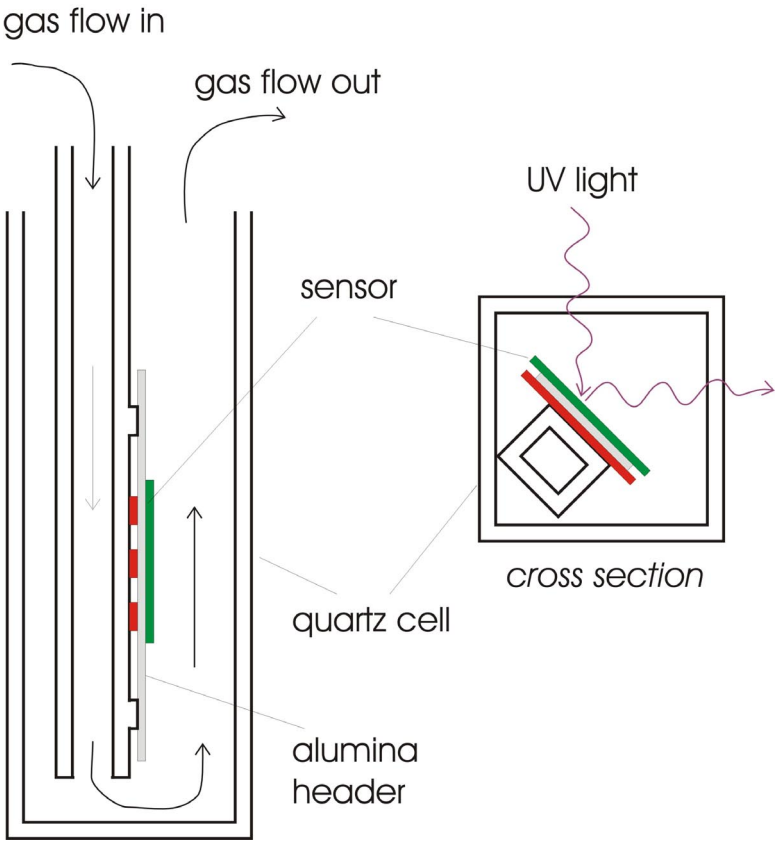


**Figure 3.9.1** Schematic of the quartz sample cell for high temperature spectroscopy in a flow-through cell, resulting in a controlled gas environment. The SiC sensor is mounted on the alumina header with backside Pt heaters (see Fig. 3.9.2) to allow for heating up to 900 K.

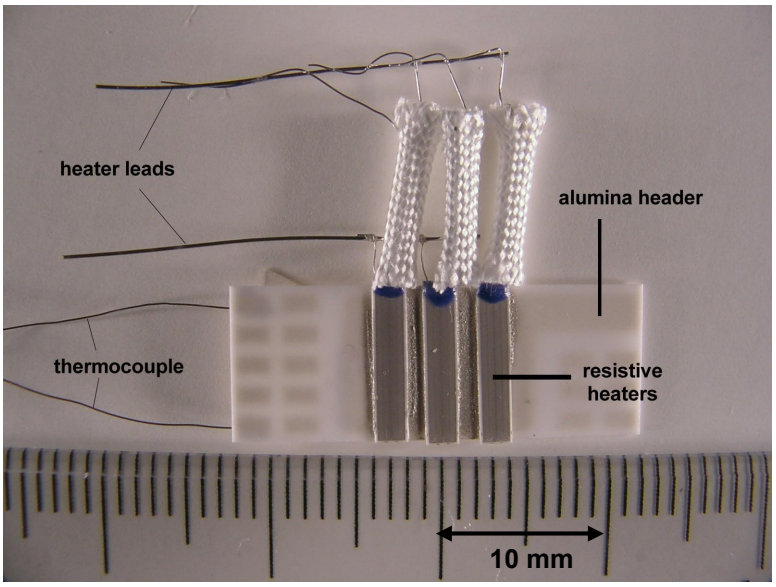


**Fig 3.9.2** Resistive microheaters on the back of the alumina header. This assembly allows us to heat the SiC sample to 900 K. The electrical connections for heaters and thermocouple are made with a microwelder. Positive and negative voltages are separated by silica insulating tubing.

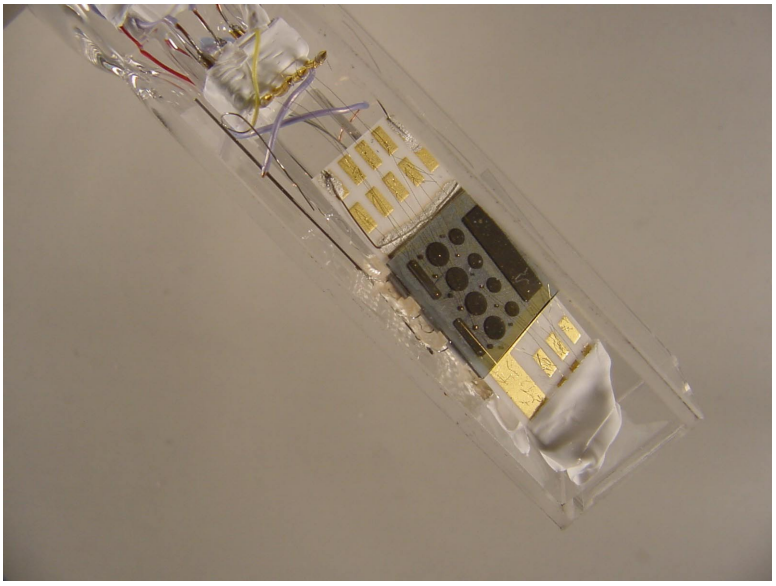

**Fig 3.9.3** Close up view of a sample on an alumina header mounted inside the gas cell. The header is held in place by the heater wires in the insulating silica tubings. Three capacitors can be electrically connected at one time. Electrical leads are provided for (1) backside Pt heaters, (2) thermocouple, and (3) three gate and one substrate contact.

**Fig 3.9.4** Photo of the assembled gas cell, for simultaneous photoemission and C-V measurements. The lower part (see Fig. 3.9.3) contains the sample and is made out of quartz for transparency in the ultraviolet.. The upper part is made out of glass, and the two parts are clamped together with a rubber O-ring in between. The electrical leads are led through the black rubber stopper on the top. The gas inlet can be seen above the clamp.

### *3.10 Oxide leakage*

To monitor the gate leakage current of our MISiC capacitors we used a Keithley 236 Source Measurement unit. All samples are first characterized with C-V curves, from which their flatband voltage can be extracted. The gate voltages of the samples is swept with typical sweep velocities of 0.1 to 1.0 V/s from positive to negative, mostly from +10 V to -10V.

### *3.11 Photoemission measurements*

For a photoemission measurement, a sample is placed in the spectrometer as described in 3.9 and then electrically connected as shown in Fig. 3.11.1. The copper wires from the gas cell have been soldered to a female connector, from microtech, Inc., whose male counterpart is fixed to the shield of the cell. The heater circuit runs on a floating battery and is electrically isolated from the signal circuit. The signal wires outside the spectrometer are connected to a battery with an adjustable resistor, allowing bias voltages from 0 to -9 V (and from 0 to +9 V with an exchange of connectors).

For a measurement series, first we close the spectrometer's light shutters and switch the signal circuit to the handheld capacitance meter, model 875B from BK Precision. This allows us to get a manual C-V curve for checking the sensor connections and extracting the actual device flatband voltage. Next the signal circuit is switched to the current preamplifier, model SRS570 by Stanford Research Systems, Inc., to check the sensor dark current at different gate bias voltages.

In the measurement series, we vary the incident wavelength, the bandwidth of the spectrometer (which effectively controls the incident UV power), and the capacitor gate bias voltage. The typical wavelength range is 200 to 260 nm (6.2 to 4.8 eV), for some measurements also higher, up to 440 nm (2.8 eV). The bandwidth of the spectrometer can be varied from 10 to 0 nm (0 meaning a closed shutter), resulting in differently shaped light spots with different light intensities. The use of larger bandwidths results in two problems: first the light spot becomes more diffuse with more of the incident photons hitting the sample outside the designated gate. Secondly, we have calibration curves for the photodiode only for the values 200 nm, 210 nm, 220 nm … These calibration values have a significant scatter, due to reflections from the glass cover above the Si detector, resulting in a non-linear relationship between sensitivity and wavelength. Therefore accurate power measurements could only be made in a small (< 2 nm) bandwidth at preset wavelengths.

In our analysis, we used only the values for bandwidths of 2, 1 and 0 nm, the last measurement serves as dark current for the other two. The capacitor gate bias voltage was changed between +1 and -6V. We have heated a sample in our sample cell to about 900 K to calibrate our thermometry, but have yet to heat a sample in the photoemission set-up itself.

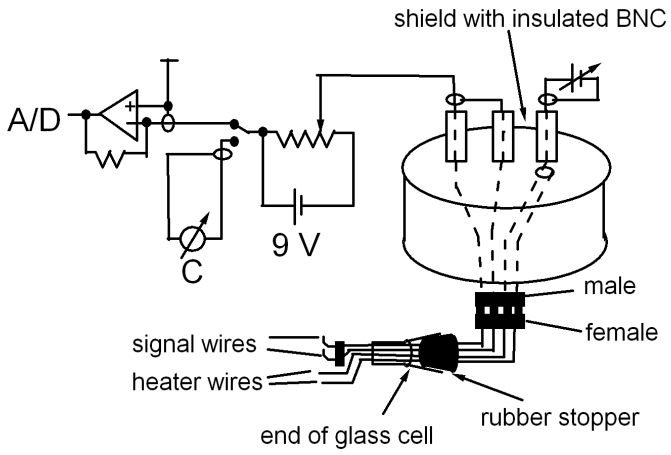


**Fig 3.11.1** Schematic of the electrical connections for a sample in the photoemission spectrometer. The sample needs two connections for the heater and two connections for the measured signals (gate and substrate). Signal and heater wires are led out of the gas cell through a rubber stopper and soldered to a female connector. From the corresponding male connector, the wires are led out of the shielded spectrometer chamber through isolated BNCs. The sample can be biased from -9 V to +9 V. By means of a switch, the operator can choose to measure either the generated sample photocurrent or the sample capacitance.

## 4. RESULTS AND DISCUSSION

In this chapter, we will present the results of our measurement, represented by some of our MISiC samples, whose parameters are given in the following table. All the analyzed devices were n-type. The bulk doping density was ~ $10^{19}$cm$^{-3}$. An ~ 5 μm epilayer was grown on the bulk, with the doping density shown in the table.

| sample | polytype | doping density ($10^{16}$ cm$^{-3}$) | oxidized by | oxide thickness (nm) | gate metals | gate area ($10^{-8}$ m$^2$) |
|---|---|---|---|---|---|---|
| A | 6H | 1.3 | Cree | 46.5 | Pt, Ti | 24.6 |
| B | 6H | 1.6 | Purdue | 43 | Pt | 5.31 |
| C | 6H | 1.6 | Purdue | 44 | Pt | 3.16 |
| D | 4H | 1.2 | Cree | 47 | Pt, Ti | 11.8 |
| E | 4H | 1.2 | Cree | 48.9 | Pt | 214 |

### *4.1 C-V measurements at temperatures up to 600 K*

Figure 4.1.1 shows the high-frequency (1 MHz) and quasi-static C-V curves of a MISiC device (sample A). For large positive gate voltages the n-type capacitor is biased in accumulation, and both curves measure the oxide capacitance. Sweeping the gate bias towards negative voltages depletes the semiconductor of majority carriers at the oxide/semiconductor interface, so the series combination of oxide plus semiconductor capacitance is measured. Since all our C-V measurements are performed in the dark, the semiconductor does not invert at large negative biases but remains in deep depletion due to the slow generation rate of minority carrier at 500 K.

The density of charged states at the oxide/SiC interface ($D_{IT}$) obtained via hi-low analysis is shown in Figure 4.1.2. For 300 K, we calculated an energy window for reliable $D_{IT}$ from 0.25 to 0.65 eV, and for 500 K from 0.55 to 1.05 eV, the energies are referenced with respect to the conduction band edge. We estimate a measurement uncertainty of about 10 %. The $D_{IT}$ for this sample is essentially constant from 0.3 to 0.7 eV. The interface state density of our devices is comparable to state-of-the-art material that is used for electronic applications [Das 2000]. SiC electronic devices typically have either Al or poly silicon gates. The measurements in Fig. 4.1.2 indicate that our use of a non-standard metal, Pt, does not adversely affect the quality of the oxide/SiC interface.

The high-frequency (1 MHz) and the quasi-static C-V curves of a second MISiC device (sample B) are shown in Fig 4.1.3. In depletion the capacitance values from the quasi-static measurements are again larger than the 1 MHz measurement, indicating the presence of interface states. Note that a few measurements points around 2 V have been so severely disturbed by current spikes, that a reliable capacitance measurement is no longer possible. Above 600 K, we find that the leakage currents of our all our devices becomes so large, that it is not possible to measure the quasi-static capacitance.

We therefore analyzed the sample interface density with an alternative technique, the Terman method that requires only high-frequency capacitance measurements. However, since the C-V characteristic in the absence of interface traps is not measured experimentally but calculated from the device parameters, the $D_{IT}$ obtained are less precise [Nicollian, 1982]. In Fig. 4.1.4 we show the interface state density obtained via both Terman and hi-low techniques for sample B. The $D_{IT}$ from the quasi-static analysis of two measurement runs agree with each other within the precision of our measurement. Note that the $D_{IT}$ obtained from the Terman method shows a systematic deviation, too small values for low energies and too high values for larger energies. The functional form of energy vs. $D_{IT}$ is an artifact of the Terman technique, as verified by Rosencher & Bois [Rosencher, 1982]. We therefore can not obtain quantitative values for interface state density using the Terman method, but can qualitatively compare the same device measured under different conditions, such as hydrogen and oxygen.

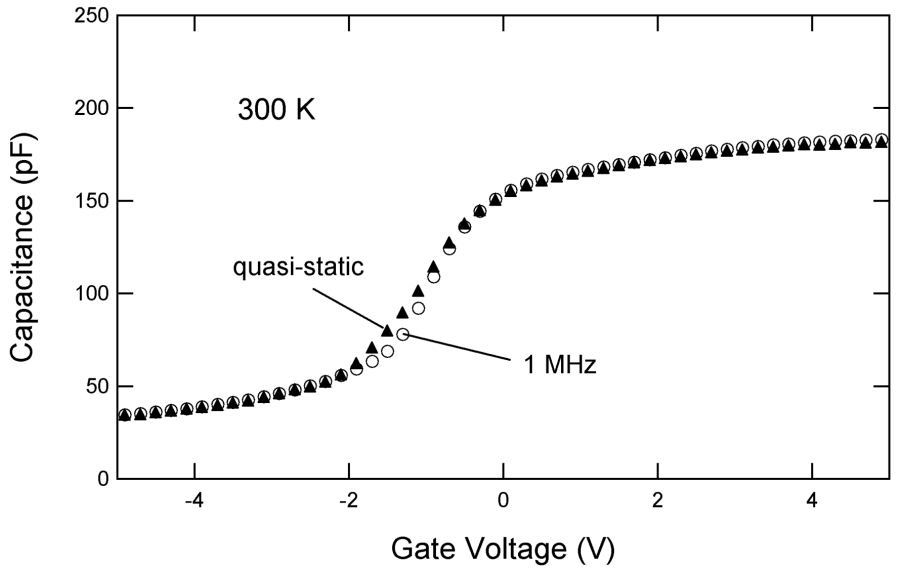


**Fig. 4.1.1**. Capacitance-voltage (C-V) curve of a MISiC device (sample A) at 300 K in air. Shown are the simultaneously measured 1 MHz and quasi-static capacitances. The gate voltage is swept from positive to negative voltages at 0.4 V/s.

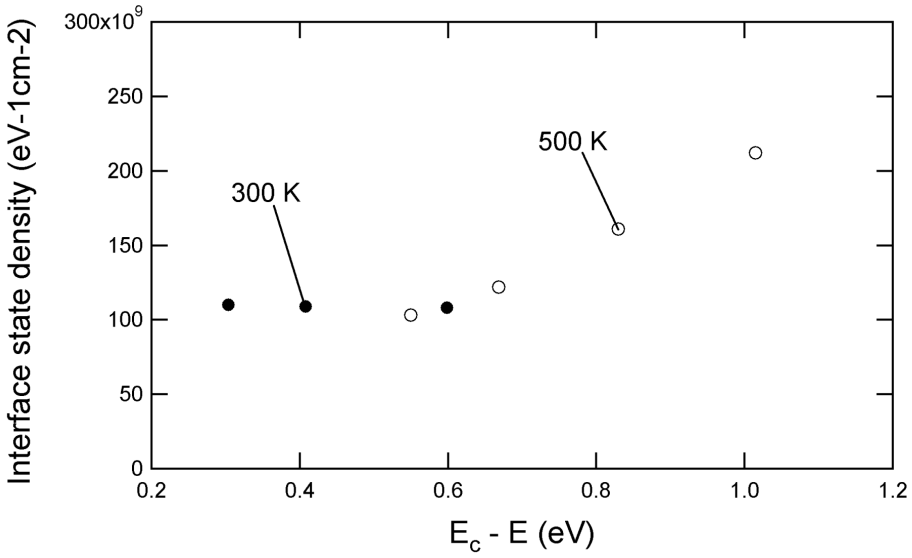


**Fig. 4.1.2** Interface state density of sample A, from hi-low analysis at 300 K (Fig. 4.1.1) and 500 K. These results are comparable to state of the art capacitors for electronic circuits with a similar gate oxide.

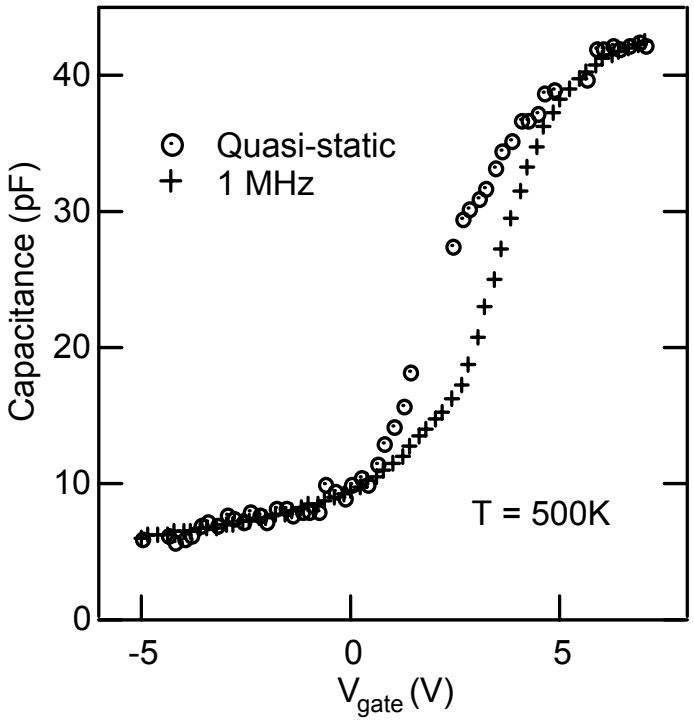


**Fig.. 4.1.3** Quasi-static and 1 MHz capacitance-voltage characteristics a MISiC device (sample B) in nitrogen at 500K. The voltage was swept from positive to negative at 0.5 V/s.

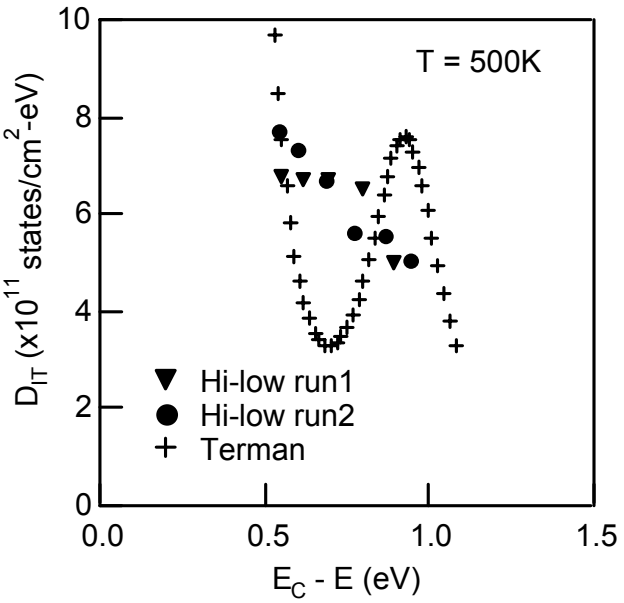


**Fig.. 4.1.4** Interface state density at 500K in nitrogen obtained from hi-low analysis (data in Figure 4.1.3) and Terman analysis of sample B. The discrepancy between the hi-low and Terman results is due to an artifact of the Terman analysis (see text).

### *4.2 C-V measurements at temperatures up to 800 K*

We have measured the C-V curve of a number of MISiC devices at temperatures above 600 K. Fig. 4.2.1 shows the C-V curve of a MISiC device (sample C) at 800 K in hydrogen and in oxygen. As expected in going from an oxidizing to reducing atmosphere, the curve in oxygen is shifted to more positive voltages than the curve in hydrogen. In oxygen the transition from accumulation to inversion is broadened compared with the curve in hydrogen. This indicates an increase in the interface state density in oxygen. Shown in Fig. 4.2.2 is the $D_{IT}$ obtained from Terman analysis of sample C in oxygen and hydrogen. As expected, over the same energy window $D_{IT}$ is larger in oxygen and hydrogen, which explains the difference in the slope of the C-V curves of Fig. 4.2.1.

Another series of high temperature (700 K) C-V measurements in hydrogen and oxygen of a different MISiC device (sample A) are shown in Fig. 4.2.3. In this case although the difference in slope between the two curves are less pronounced, the curve in oxygen is again broader than the curve in hydrogen. Within our measurement accuracy, the 1 MHz C-V characteristic in hydrogen at 700 K, is what we would obtain for an ideal MISiC device with no interface states. The measurements shown in Figs. 4.2.1 and 4.2.3, indicate that for temperature above 700 K the presence of oxygen results in the creation of charged defects at the oxide/SiC interface, whereas hydrogen reversibly passivates these defects. These effects were found in all of the samples we investigated, in devices fabricated on both the 6H and 4H polytypes, independent of the specific details of both oxidation and metallization [Ghosh 2003]. We conclude that the observed passivation and activation of defects in hydrogen and oxygen is intrinsic to silicon carbide field-effect structures, independent of the specific details of device fabrication.

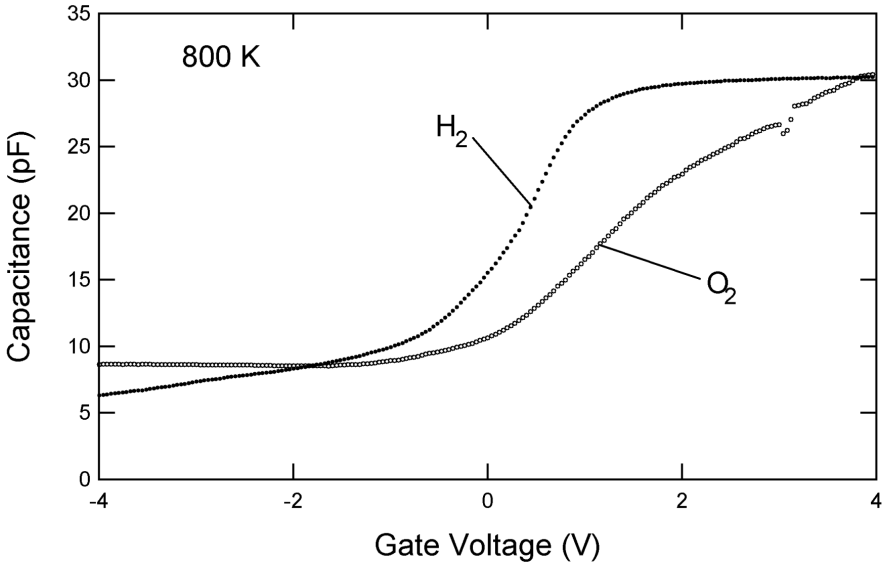


**Fig. 4.2.1** C-V curves of sample C at 800 K in reducing gas (10 % $H_2$ in $N_2$) and oxidizing gas (1 % $O_2$ in $N_2$). Operation in a reducing environment results in both a flat band shift (standard sensor response) and reversible annealing of charged states at the $SiO_2$/SiC interface. The voltage is swept from positive to negative with 0.09 V/s.

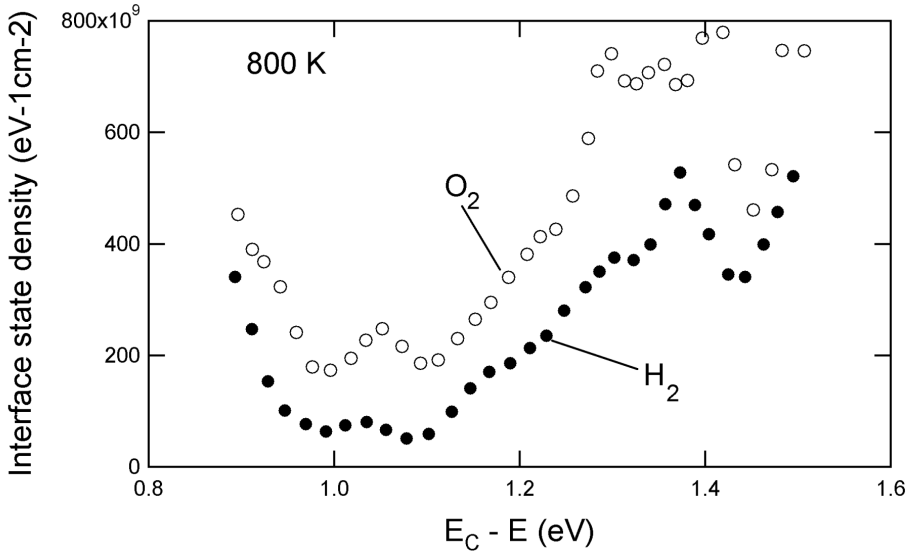


**Fig. 4.2.2** Interface state density of sample C, at 800 K in 1% oxygen and 10% hydrogen environment (balance gas is nitrogen) calculated using the Terman method. The energy window extends at this temperature from 0.9 to 1.5 eV.

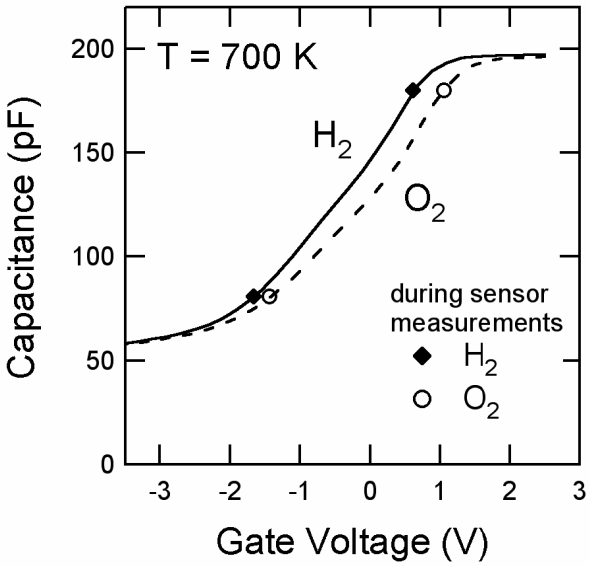


**Fig. 4.2.3** High frequency capacitance of sample A, measured in two gas environments, 10% $H_2$ in $N_2$ and 1% $O_2$ in $N_2$. The gate voltage is swept from positive to negative voltages at 0.15 V/s, and the high frequency is 1 MHz. Also indicated are the gate voltages during two separate sensor measurements (see Fig. 4.3.1) where the capacitance was held at a constant value of 80 pF and 180 pF, respectively.

### *4.3 Sensor measurements*

Extensive sensor measurements were performed on sample A, and are shown in Figs. 4.2.3, 4.3.1 and 4.3.2. During sensor measurements, the capacitance is held constant while changing the gas environment; and the corresponding gate voltage is recorded as the sensor signal. The difference in voltage depends on the chosen capacitance set point, with larger responses for larger capacitances, as seen in Fig. 4.2.3. There, we have indicated the measured gate voltages during two sensor measurements with symbols. At 180 pF the sensor response to a change from hydrogen to oxygen is 0.44 V, while at 80 pF the response is only 0.23 V.

Fig. 4.3.1 shows the two sensor measurements at 180 and 80 pF, taken after the C-V traces of Fig. 4.2.3. Each measurement consists of two cycles between hydrogen and oxygen, with short exposures to pure nitrogen in between. For comparison, the sensor is exposed to oxygen in both measurements at a time of around 80 min. Initially, both responses are fast with a similar increase of the gate voltage and a time constant of ~1 min, but then the sensor at 180 pF continues to increase slowly with a time constant of ~40 min. This makes the use of the sensor at 180 pF impractical. The sensor response at 180 pF is 0.44 V, including the slow tail in oxygen. The total sensor response at 80 pF is only 0.23 V but reaches saturation faster. Note that the asymptotic values of the sensor signal from Fig. 4.3.1 in both hydrogen (diamond symbols) and oxygen (circle symbols) are overlaid on the original C-V curve in Fig. 4.2.3. The measured gate voltages between C-V characteristics and sensor measurements agree within 30 mV.

Fig. 4.3.2 demonstrates that the effect of gas exposure on the device's C-V characteristic is reversible. We show the C-V curves in hydrogen prior to making the sensor measurement of Fig. 4.3.1, and after four hours of cycling between oxygen and hydrogen. The device was allowed to equilibrate for 15 minutes in hydrogen prior to each measurement. The differences between the values before and after are below 1% of the maximum capacitance value. We have chosen to make this measurement in hydrogen, because the sensor takes a very long time to equilibrate in oxygen (see the upper panel of Fig. 4.3.1).

The response of MISiC sensors to hydrogen containing gases has been attributed to date solely to the formation of a polarized layer at the metal-$SiO_2$ interface [Lloyd Spetz, 1997], which occurs following a reduction of the metal-$SiO_2$ work function difference in hydrogen [Lundström 1976]. This "classic" sensor response mechanism accounts for only a portion of the observed sensor responses according to the model we present in Fig. 4.3.3.

Our model shows the charge distribution in the sensor that we assume for different gas atmospheres [Tobias 2003A]. For a MISiC device biased at constant capacitance, the potentials in the silicon carbide are constant, regardless of gas exposure. In a hydrogen atmosphere, hydrogen dissociates at the metal surface and diffuses relatively quickly into the sensor. Diffusion times less than 5 μs in the platinum gate are calculated from [Katsuta 1979], and times less than 0.5 ms in the $SiO_2$ layer are calculated from [Beadle 1985]. A polarized layer then builds up at the metal-$SiO_2$ interface with the protons in the $SiO_2$ and the electrons in the metal. The dipole moment per hydrogen atom is larger than 2 Debye [Fogelberg, 1997], indicating a separation of the positive and negative charge densities of the hydrogen. When the polarized layer has

built up, the potential of the platinum decreases in hydrogen, according to Poisson's equation.

In an oxygen atmosphere, the hydrogen reacts with oxygen on the metal surface and is thereby removed from the sensor. The disappearance of the polarized layer at the metal-$SiO_2$ interface increases the potential of the platinum. The disappearance of the polarized layer, however, cannot be the only effect of oxygen, because this would lead only to a parallel shift of the C-V curve towards higher voltages and not to a shape change of the C-V curve in Figs. 4.2.1 and 4.2.3. The shape is influenced by the density of electronic states at the insulator semiconductor interface, because the states can partly screen the influence of the gate voltage on the semiconductor. As the interface state density increases, the transition between accumulation to inversion requires a larger change in gate voltage and the slope of the C-V curve in depletion decreases. In oxygen, the C-V curve has a smaller slope than in hydrogen, indicating a higher density of defects at the $SiO_2$-SiC interface. To explain the changing shape of the C-V curve, we assume that hydrogen can passivate defects at the interface as indicated in our model in Fig. 4.3.3. Such a passivation is generally believed to be the reason of the effectiveness of the last hydrogen anneal of silicon field-effect components that need low interface state densities [Pierret, 1990]. In oxygen, hydrogen leaves the charged states it has been passivating. The states that lie below the Fermi level then become filled with electrons, as seen by the direction of the sensor response. We also see that the defects behave as acceptors. A major difference between devices based on silicon and devices based on silicon carbide is that the latter can operate at temperatures where hydrogen passivation or hydrogen removal takes place.

The model can explain the different sensor responses for different pre-set values of the capacitance, shown in Fig. 4.3.1. At a pre-set capacitance value of 180 pF the Fermi level is closer to the conduction band than at a value of 80 pF. The interface state density in our samples is larger near the conduction band edge than at midgap [Ghosh 2002, 2003], similar to that observed in silicon [Nicollian 1982, p. 293]. Therefore, at 180 pF more defects take up an electron during oxygen exposure than at 80 pF. This makes the response at 180 pF larger; however, the additional portion of it is also slower. The portion of the response due to the work function has the same magnitude and time constant for any capacitance value. We believe that the slow response of the defects is due to the slow desorption of hydrogen from defects it has been passivating. We cannot measure the fast component of the Pt-$SiO_2$ interface response to hydrogen, because the gas exchange time of our current measurement system is too slow. We are currently building a system for measuring response times in the millisecond range [Tobias, 1999]. For most sensor measurements, the slow part of the sensor response is to be avoided.

What capacitance set point should be chosen for optimum sensor performance? The choice of capacitance set point determines the position of the Fermi level in the SiC band gap at the $SiO_2$-SiC interface, and the position of the Fermi level determines which kind and how many defects will take up or release electrons during oxygen exposure. In the $SiO_2$- SiC system, the defect density decreases as the Fermi level is swept from the conduction band edge to midgap. When the Fermi level is near mid gap, see Fig. 4.3.4, the contribution due to interface states with long time constants are reduced and the work function change dominates the sensor response, as shown in Fig. 4.3.1. The precise value of the interface state density is very sensitive to oxidation conditions and post oxidation

processing parameters [Pierret, 1990]. In order to obtain repeatable results from independently fabricated devices, the effect of these states needs to be minimized.

A second criterion is minimizing the gate leakage current, large leakage currents usually result in short device lifetimes. When the sample is biased near midgap, the SiC near the insulator is depleted of electrons, therefore only a few electrons will be injected from the SiC into the insulator. On the other hand for gate biases near and above flatband, electron injection is much larger. It has been shown that as gate leakage currents decrease the high temperature lifetime of SiC field-effect structures increases [Maranowski 1998]. Therefore, we propose that the optimum bias point in terms of sensor response time, sensor-to-sensor repeatability and long-term sensor stability is near midgap.

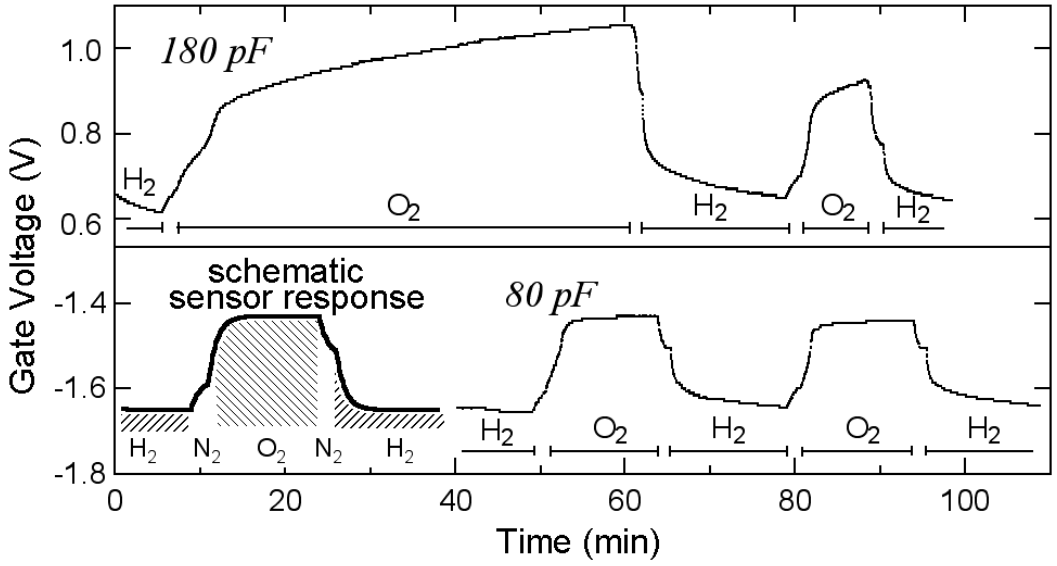


**Fig. 4.3.1** Sensor measurements on sample A shown in Fig. 4.2.3 at 700 K, the capacitance is held constant and the gate voltage is recorded as sensor signal during the gas exchanges. The measurement sequence is shown schematically in the lower left curve: the sensor is exposed to 10% $H_2$ in $N_2$ and 1% $O_2$ in $N_2$, separated by a short exposure to pure nitrogen. We observe a reversible increase in $O_2$ and decrease in $H_2$. In the upper half of the figure the capacitance is kept at 180 pF, in the lower half at 80 pF.

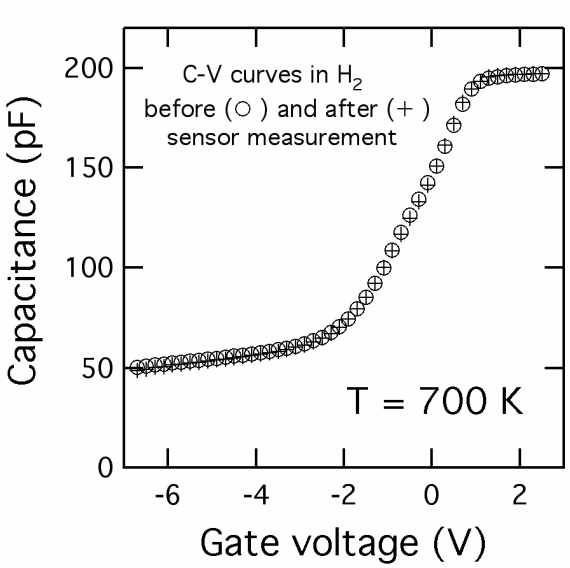


**Fig. 4.3.2** C-V characteristic of the sensor shown in Fig. 4.2.3 (sample A), showing that the effects of gas exposure are reversible. The device was allowed to equilibrate in a hydrogen environment for 15 minutes prior to each measurement. The initial C-V curve in $H_2$ is well reproduced after four hours of cycling between $O_2$ and $H_2$ at 700 K.

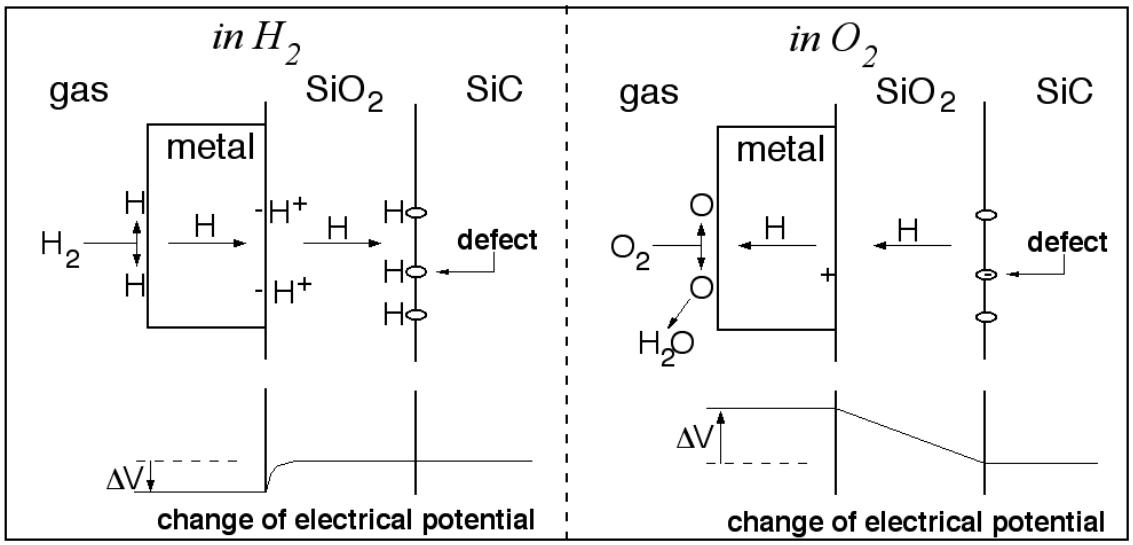


**Fig. 4.3.3** Distribution of charges in the MISiC sensor during exposure to $H_2$ (left) and $O_2$ (right), respectively. When the sample capacitance is kept constant, the charge distribution and the potentials inside the SiC do not change. During $H_2$ exposure, hydrogen atoms and molecules diffuse into the sample. Some adsorb at the metal-$SiO_2$ interface with the protons in the $SiO_2$ and the electrons in the metal, other adsorb at the $SiO_2$-SiC interface where they passivate interface states and prevent them from charging. The charge distribution at the metal-$SiO_2$ interface decreases the potential of the metal, and, therefore, the gate voltage decreases in $H_2$. During $O_2$ exposure, the hydrogen in the sample is consumed at the metal surface. The states at the $SiO_2$-SiC interface can now be negatively charged, and the compensating positive charge is in the metal. The potential of the metal increases and, therefore, the gate voltage increases in $O_2$.

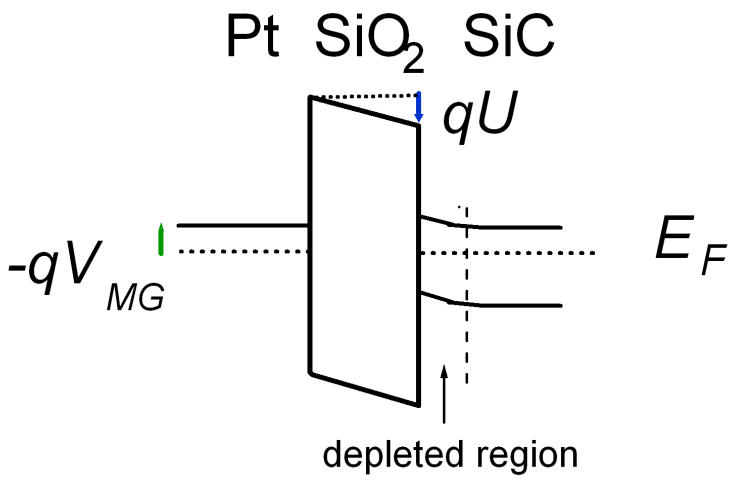


**Fig. 4.3.4** Band diagram of a MISiC sample at midgap. $E_F$ is the Fermi level in the SiC, $V_{MG}$ the gate voltage applied at midgap, and $U$ the voltage drop over the insulator $SiO_2$. At this bias the fields in the oxide are close to zero so the leakage current through the oxide is comparatively small. For high temperature operation biasing at mid-gap increases the device lifetime.

### *4.4 Leakage Measurements*

Long-term stability of MISiC sensors requires low gate leakage currents. Additionally, the photoemission measurements, to be described in section 4.5, can only be performed when the leakage current is less than the photo generated current. We have therefore, started to characterize the leakage current of our devices as a function of bias voltages and temperature. Fig 4.4.1 shows an example of these measurements on sample D. In a typical sample with an array of gates (see Fig. 3.6.2), about two-thirds or more of them have low leakage currents when biased in inversion. However, only a few of the devices have a leakage current less than 5 pA over the entire bias voltage range at room temperature. All such devices have gate areas below 2 x $10^{-7}$ $m^2$. This may be, because many small insulator defects are distributed over the silicon carbide surface, such that there is a high probability that a device with a large area gate ends up with at least one defect. To test this hypothesis, we plan further leakage measurements along with statistical analysis to correlate the magnitude of the leakage current with the gate area.

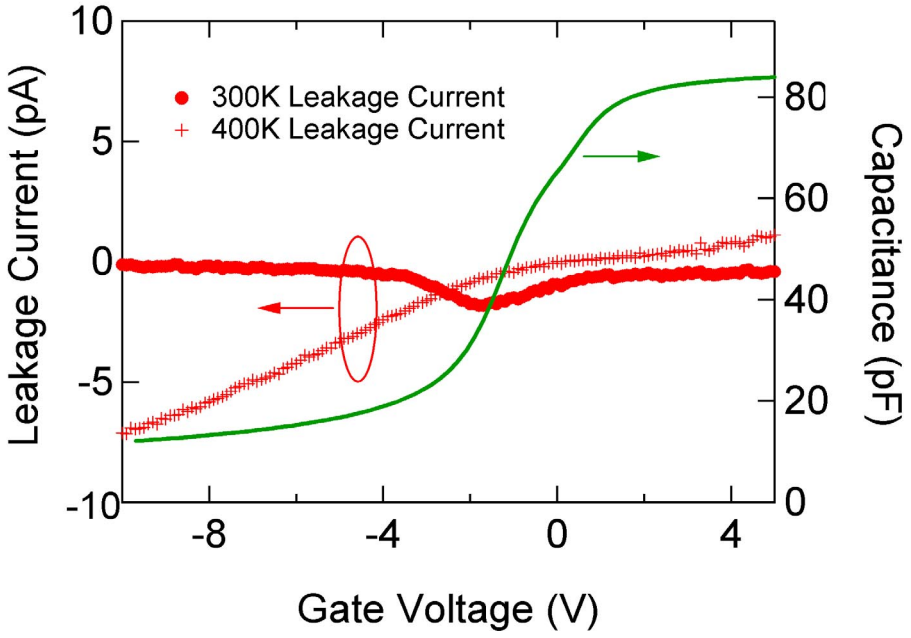


**Fig 4.4.1** Leakage currents in a MISiC (sample D) at 300 K (●) and at 400 K (+). The flatband voltage is -0.6 V as seen from the C-V curve at 300 K (—). The voltage was swept from positive to negative with 1 V/s. The leakage current at 300 K is close to our measurement resolution, whereas at 400 K the current increases in inversion.

### *4.5 Photoemission measurements – extraction of the chemically induced barrier height*

*Theory - Photoemission*

Capacitance measurements alone give us an incomplete picture of what is happening in the MISiC device during exposure to hydrogen and oxygen. We show in Figs. 4.51 and 4.5.2 schematic band diagrams of our MISiC capacitors to explain how the C-V curves are modified by the presence of hydrogen or oxygen. At the flatband voltage, the bands in the semiconductor are constant with respect to position. The reference energy for electrons in our devices is taken to be the silicon carbide Fermi level, EF. The applied voltage, VFB, is the difference between the reference energy and the Fermi level in the platinum divided by the electronic charge, q. The energy difference between the Fermi level in the platinum and the conduction band in the insulator is called E. The energy difference, F, between EF and the insulator conduction band is assumed independent of gas exposure.

In hydrogen, Fig. 4.5.1, the interface state density at the silicon carbide-insulator interface is essentially zero, to within our experimental uncertainty, whereas in oxygen it is measurable [Ghosh, 2002; Ghosh, 2003]. $D_{IT}$ is small at midgap and increases towards the conduction band edge. During oxygen exposure the negatively charged interface states, shown in Fig. 4.5.2, are compensated by positive charge in the metal. This leads to an electric field in the insulator during oxygen exposure, even at flatband conditions in the silicon carbide, and a resulting voltage drop, $U$. From the band diagram, we deduce, with positive voltages pointing downwards:

$$-qV_{FB} = F + (-qU) - E \qquad (1)$$

The voltage drop across the insulator, $U$, depends on the density per unit area of accessible defects, $n$, at the insulator- silicon carbide interface below and within $kT$ of $E_F$. It can be expressed in terms of the insulator thickness, $t$, the dielectric constant of the insulator, $\varepsilon$, and $q$:

$$U = nqt / \varepsilon \qquad (2)$$

When the gas environment of the device is changed from hydrogen to oxygen, the resulting change, $\Delta V_{FB}$, of $V_{FB}$ can be related to the changes, $\Delta E$ and $\Delta n$, of $E$ and $n$, respectively ($F$ is constant).

$$\Delta V_{FB} = \Delta nqt / \varepsilon + \Delta E / q \qquad (3)$$

As the gas is changed from hydrogen to oxygen it has been shown that $E$ increases [Lundström, 1976]. $n$ increases as well because of the creation of charged states at the insulator-silicon carbide interface [Ghosh, 2002]. With both $E$ and $n$ increasing in oxygen, $V_{FB}$ must also increase, as seen in Fig. 4.5.2.

The effect of the change from hydrogen to oxygen on $E$ is independent of the possible band bending in the silicon carbide. Therefore, in Fig. 4.2.3, the increase of $E$ in oxygen is the same for all measurement points and would, without interface states, lead to a parallel shift of the C-V curve along the voltage axis. On the other hand, the density of

accessible defects, *n*, is larger when the Fermi level is close to the conduction band. The effect of the change from hydrogen to oxygen on *E* is independent of the possible band bending in the silicon carbide. This leads to the larger increase of the gate voltage in oxygen for higher capacitances, as seen in Figs. 4.2.1 and 4.2.3.

To distinguish between the effect of $\Delta n$ and $\Delta E$, we have set up the photoemission experiment to measure $\Delta E$ alone, for which the band diagram is shown in Fig. 4.5.3 [Tobias 2003B]. In this experiment, we will generate a photocurrent, *I*, over the metal-insulator-barrier that depends on difference of photon energy, *hf*, and the barrier height, *E* [Lundström 1976; Sze 1981]. The dependence is theoretically quadratic, but sometimes it is observed to be closer to cubic [Sze, 1981]. By plotting the square root of the photocurrent as a function of energy, the barrier height can be obtained from the intercept of the linear portion of the data. As shown in Fig. 4.5.3, for our n-type capacitors the device needs to be biased in accumulation to collect all the photogenerated electrons via the substrate contact.

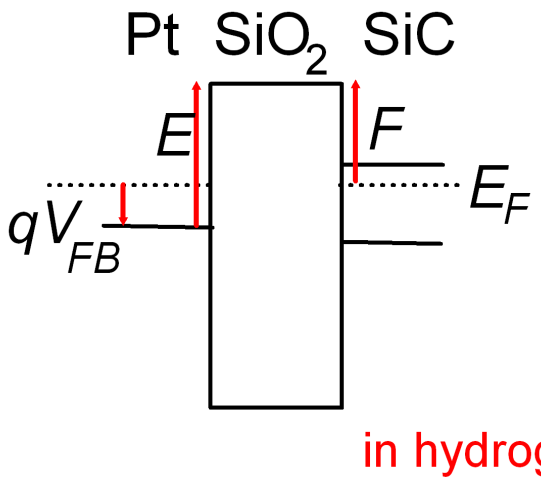


**Fig. 4.5.1** Band diagram of a MISiC at flatband in hydrogen. The defect density at the $SiO_2$/SiC interface of $SiO_2$ is assumed to be negligible. The barrier height, E, is smaller than in oxygen.

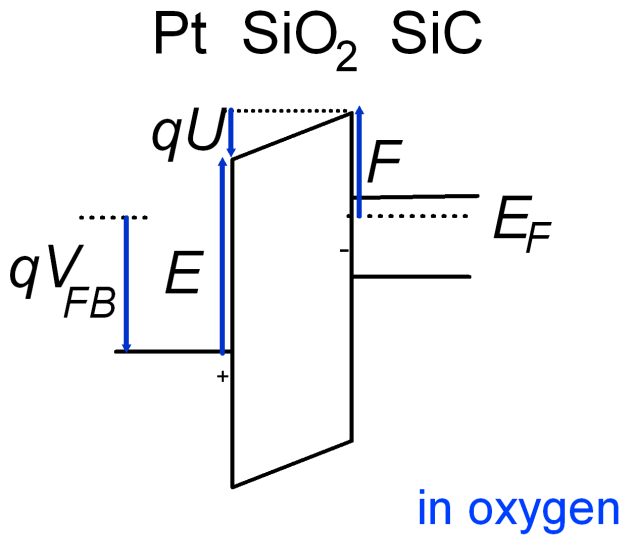


**Fig. 4.5.2** Band diagram of a MISiC at flatband in oxygen. The defect density at the $SiO_2$/SiC interface gives rise to a voltage drop, U, in the insulator. Compared to the hydrogen case, the barrier height, E, increases along with U. Therefore, only the sum of the changes in U and E can be determined in capacitance measurements.

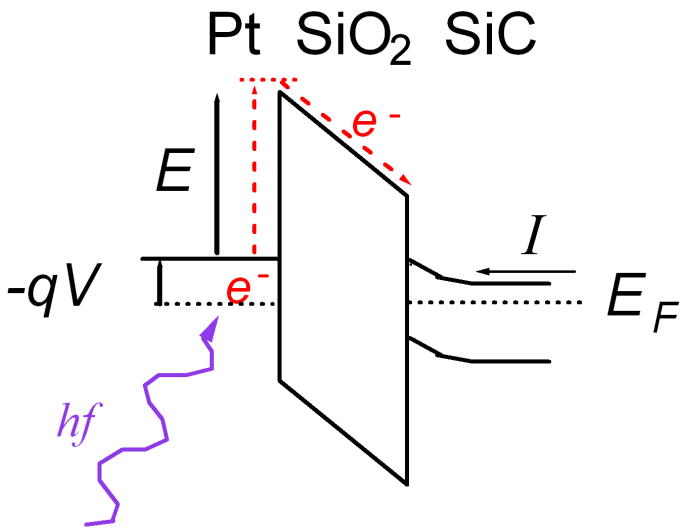


**Fig. 4.5.3** Band diagram of a MISiCs device (sample E) during the photo emission measurement. Photons with energy, hf, excite electrons in the metal to move to a higher state and then over the metal-insulator barrier. The photocurrent, I, depends only slightly on the bias voltage V but strongly on the height of the barrier, E:

$$I \sim (hf - E)^n \quad \text{with } 2 \leq n \leq 3$$

*Experiment - Photoemission*

Photoemission measurements were obtained from an n-type capacitor with 15 nm Pt gates (sample E), see Fig. 4.5.4. A large gate with dimensions of 0.7 mm x 3 mm (see Fig. 3.9.3) was chosen to match the spatial extent of the ultra-violet light spot with the gate area. Fig. 4.5.4 shows the square root of the photocurrent as a function of incident photon energy. As expected from theory the photo current decreases with decreasing energy, approaching an asymptotic value, which represents the barrier height. The barrier height, E, between platinum and silicon dioxide can be estimated to first order as 4.7 eV, by using the difference in the work function of platinum (~5.7 eV) [CRC, 1996] and the electron affinity of silicon dioxide (~1 eV) [Nicollian, 1982, p. 464]. The excitation energy for the photoemission measurements was chosen to be 4.85 - 5.9 eV (210 nm - 255 nm), in order to ensure that the photoexcited electrons can surmount the 4.7 eV barrier. In order to excite electrons to a high energy state near the metal-insulator interface we fabricated capacitors with thin (15 nm) metal gates. Using the extinction coefficient for platinum at 5 eV, we obtain a penetration depth of 12 nm [CRC, 1996, p.12-138].

In order to extract the barrier height from the data in Fig. 4.5.4, we need to normalize the photocurrent measured at each photon energy for the number of photons that arrive at the metal - oxide interface. First, we correct the measured currents for the dark current, which is in the order of 10 pA (the noise in the measurements is about 5 pA). Second, we correct for the spectral output of the Xe lamp, i.e. that the number of photons incident on the sample is a function of wavelength. A third issue, which we have not yet taken into account is that the reflectivity of the Pt gate depends on the photon energy. This will require simultaneously measurements of the photocurrent and reflectivity. As evident from the data, even at an incident photon energy of 4.7 eV, the photocurrent for a given gate bias does not depend linearly on the incident photon energy. Further measurements are needed at lower energies to extrapolate an intercept. An additional issue that we need to account for is the observed gate bias dependence of the photocurrent. The gate bias voltage, *V*, should only indirectly influence the photocurrent by decreasing the barrier height through the Schottky effect. We calculate that the image charge lowering of the barrier height is 0.1 eV x $(V_{flatband} - V_{gate})^{1/2}$. The data in Fig. 4.5.4 has too strong a dependence on gate bias voltage to be explained solely with the Schottky effect.

We have fabricated a quartz sample cell that will allow us to make simultaneous capacitance – voltage and photoemission measurements at temperatures up to 900K in a controlled gas environment. Preliminary measurements demonstrate that our n-type capacitor samples have low enough gate leakage currents to measure the photo induced gate to substrate current. As expected from theory the photocurrent decreases with decreasing photon energy, approaching an intercept that is a measure of the chemically induced barrier height. We have identified the experiments that will need to be performed to extract quantitative values of the barrier height from the measured data. The photoemission technique will allow us to measure quantitatively the chemically induced change in the metal/semiconductor barrier height as a function of gas composition and temperature.

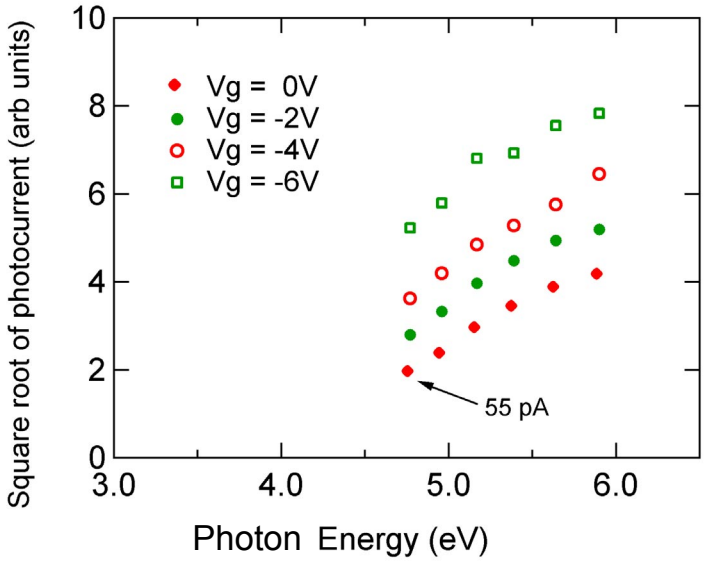


**Fig 4.5.4** Photoemission data of a MISiC device (sample E) under different bias voltages. Shown is the square root of the photocurrent. At each photon energy, the photocurrent has been corrected for variations in light intensity and dark current. As expected from theory, the device photocurrent decreases with decreasing incident photon energy, approaching an asymptotic value that represents the metal - semiconductor barrier height.

## 5. CONCLUSIONS

Prior to our *in-situ* characterization of the electronic properties of MISiC sensors, it was assumed that the response of these devices to hydrogen containing gases was due simply to the chemically induced shift in the metal/semiconductor barrier height. We have found that at temperatures above 600 K an additional phenomena: the passivation and activation of states at the insulator-silicon carbide interface, is also present. These two phenomena were found to be present in all of the devices we have studied, regardless of the SiC polytype as well as specific oxidation and sensor fabrication parameters. Understanding the physical origin of the hydrogen mediated passivation of charged interface states is important for the operation of any type of MISiC sensor because the time constant for this phenomena can be significantly longer than the "classic" response mechanism. In order to separate the effects of the two phenomena we have built a set up to characterize the same sample via both *in-situ* capacitance - voltage and *in-situ* photoemission spectroscopy.

We concluded that the best operating point for MISiC devices during sensor measurements is close to midgap, from the energy distribution of the gas induced charged defects. At this bias the chemically induced barrier height shift dominates, and the effect of interface states is minimized. An additional benefit of biasing the sensor at midgap is the anticipated increase in sensor to sensor reliability at high temperature.

REFERENCES


[Beadle 1985] W. E. Beadle, J. C. Tsai and R. D. Plummer, *Quick Reference Manual for Si Integrated Circuit Technology,* 6-34, Wiley, New York (1985).

[Cooper 1997] J. A. Cooper, Jr., "Advances in SiC MOS Technology", Phys. Stat. Sol. A **162**, 305-320, (1997).

[CRC 1996] CRC Handbook of Chemistry and Physics, p. 12-122, and p. 12-138, CRC Press, ISBN 0-8493-0477-6 (1996).

[Cree] Cree Research Inc., Durham, NC 27703, USA.

[Das 2000] M. K. Das, B. S. Um and J. A. Cooper, Jr., "Anomalously High density of Interface States Near the conduction Band in SiO2/4H-SiC MOS Devices", Mat. Sci. Forum, **338-342**, 1069-1072, (2000).

[Filippov 1999] V. I. Filippov, A. A. Vasilev, A. A. Terentev, W. Moritz and U. Roth, "Sensor Based on a Pt/LaF3/$SiO_2$/SiC Structure for the detection of chlorofluorocarbons", Tech. Phys. **44**, 1334-1339 (1999).

[Fogelberg, 1997] J. Fogelberg, M. Eriksson, H. Dannetun, and L.-G. Petersson, "Kinetic modeling of hydrogen adsorption/absorption in thin films on hydrogen-sensitive field-effect devices: Observation of large hydrogen-induced dipoles at the Pd-SiO2 interface", J. of Appl. Phys., **78**, 988, 1997.

[Ghosh 2002] R. N. Ghosh, P. Tobias, S. Ejakov and B. Golding, "Interface States in High Temperature SiC Gas Sensing", Proc. IEEE Sensors 2002, **2**, 1120-1125, paper 6-4 (2002).

[Ghosh 2003] R. N. Ghosh, P. Tobias and B. Golding, "Influence of interface states on high temperature SiC sensors and electronics", *in SiC - Material, Processing and Devices 2002*, Mat. Res. Soc. Symp. Proc. **742**, paper K7.5 (2003).

[Hunter 2000] G. W. Hunter, P. G. Neudeck, M. Gray, D. Androjna, L.-Y. Chien, R. W. Hoffman, Jr., C. C. Liu and Q. H. Wu, "SiC-based Gas Sensor Development', Mater. Sci. Forum **338-342**, 1439-1422 (2000).

[Katsuta 1979] H. Katsuta ad R. B. McLellan, J. Phys. Chem. Solids, "Diffusivity, Permeability and Solubility of Hydrogen in Platinum", **40**, 697-699, (1979).

[Kim 2001] C. K. Kim, J. H. Lee, S. M. Choi, I. H. Noh, H. R. Kim, N. I. Cho, C. Hong and G. E. Jang, "Pd and Pt SiC Schottky Diodes for Detection of $H_2$ and $CH_4$ at High Temperature", Sensor. Actuat. B-Chem. **77**, 455-462 (2001).

[Lipkin 1996] L. A. Lipkin and J. W. Palmour, "Improved Oxidation Procedures for Reduced $SiO_2$/SiC Defects", J. Electron. Mater., **25**, 909-915, (1996).

[Lloyd Spetz, 1997] A. Lloyd Spetz, A. Baranzahi, P. Tobias, I. Lundström, "High temperature sensors based on metal insulator silicon devices", Phys. Stat. Sol. A , **162**, 493-511, 1997.

[Lundstrom 1976] I. Lundström and T. DiStefano, "Influence of Hydrogen on Pt-$SiO_2$-Si Structures", Sol. St. Comm. **19**, 871-875 (1976).

[Maranowski 1998] M. M. Maranowski and J. A. Cooper, Jr., "Time-Dependent-Dielectric-Breakdown Measurements of Thermal Oxides on N-Type 6H-SiC", IEEE Trans. Electron. Devices, **46**, 520-524 (1998).

[Nakagomi 2001] S. Nakagomi, Y. Shindo, and Y. Kokubun, "Stability of electrical properties of high-temperature operated H-2 sensor based on Pt-I-SiC diode" Phys. Stat. Solidi A **185**, 33-38 (2001).

[Nicollian 1982] E. H. Nicollian and J. R. Brews, *MOS Physics and Technology*, Wiley, New York, 1982, pp. 321-333 and 383-404.

[Palik 1985] ] E. D. Palik, *Handbook of Optical Constants of Solids,* Academic Press, London, ISBN 0-12-544420-6, 1985.

[Pierret, 1990] R. F. Pierret, Field effect devices, Addison-Wesley Publishing Company, 2nd ed., p. 95-115, ISBN 0-201-12298-7, 1990.

[Rosencher 1982] E. Rosencher and D. Bois, "Comparison of Interface State Density in MIS Structure Deduced from DLTS and Terman Measurements", Electron. Lett., **18**, 545-546, (1982).

[Samman 2000] A. Samman, S. Gebremariam S, L. Rimai L, X. Zhang, J. Hangas and G. W. Auner, "Silicon-carbide MOS Capacitors with Laser-ablated Pt Gate as Combustible Gas Sensors", Sensor. Actuat. B-Chem. **63**, 91-102 (2000).

[Serina 2001] F. Serina, K. Y. S. Ng, C. Huang, G. W. Auner, L. Rimai and R. Naik, "Pd/AlN/SiC Thin-film Devices for Selective Hydrogen Sensing", Appl. Phys. Lett. **79**, 3350-3352 (2001).

[Silverprint] Silverprint, containing silver powder and organic solvents, GC electronics, Rockford, IL 61102-2690, USA

[Spetz 2001] A. Lloyd Spetz, L. Unéus, H. Svennningstorp, P. Tobias, L. G. Ekedahl, O. Larsson, A. Göras, S. Savage, C. Harris, P. Mårtensson, R. Wigren, P. Salomonsson, B. Häggendahl, P. Ljung, M. Mattsson and I. Lundström, "SiC Based Field Effect Gas Sensors for Industrial Applications", Phys. Stat. Solidi A **185**, 15-25, (2001).

[Sze 1981] S. M. Sze, Physics of semiconductor devices, Wiley, p. 395-397, ISBN 0471-05661-8 (1981).

[Terman 1962] L. M. Terman "An Investigation of Surface States at a Silicon/Silicon Oxide Interface Employing Metal-Oxide-Silicon Diodes", Solid-State Electron., **5**, 285-299 (1962).

[Tobias 1999] P. Tobias, P. Martensson A. Goras, I. Lundström, A. Lloyd Spetz, "Moving gas outlets for the evaluation of fast gas sensors", Sens. Actuat. B. **58**, 389-393, (1999).

[Tobias 2003A] P. Tobias, B. Golding and R. N. Ghosh, "Interface states in high-temperature gas sensors based on silicon carbide", invited issue of IEEE Sensors Jour. **2**, 543-547, (2003).

[Tobias 2003B] P. Tobias, G. Golding and R. N. Ghosh, "Sensing Mechanisms of high temperature silicon carbide field-effect devices", Transducer 2003, paper 2E4.P (2003).

BIBLIOGRAPHY
None

LIST OF ACRONYMS AND ABBREVIATIONS

SiC – silicon carbide

$SiO_2$ – silicon dioxide

MISiC – metal insulator silicon carbide (device)

Quasi-static – calculated C-V from the charge flowing onto a sensor at each voltage step